Surface-confined core–shell structures based on gold nanoparticles and metal–organic networks†

Revital Kaminker,[a] Michal Lahav,[a] Marc Altman,[a] Guennadi Evmenenko,[b] Pulak Dutta,[b] Antonino Gulino[c] and Milko E. van der Boom*[a]

Here we show a step-wise approach for the formation of continuous shell-structures on surface-confined gold nanoparticles. The nanoparticle-cores induce order in the shell-structure, which consists of metal–organic networks. Communication between the organic and inorganic parts is reflected in their optical properties.

The formation of molecular thin films has been the focus of extensive research efforts directed towards the design of organic-based devices.[1] The combination of organic films and inorganic materials such as metallic nanoparticles (NPs) can result in synergistic effects and new materials that possess functions that are not attainable with single-component systems.[2–4] The *a priori* design of organic–inorganic materials with control over their composition, structure, and function is challenging because many factors are involved, for example, weak intermolecular forces, substrate morphology, and dielectric media.[5] Combining metallic NPs with organics has led to hybrid materials with interesting and useful properties.[6a] For example, surface plasmonic effects of metallic nanoparticles on the performance of polymer-based solar cells have been reported.[2a,6b] Moreover, the localized surface plasmon resonance (LSPR) of metallic nanostructures is known to be highly sensitive to its environment and has been used for detecting various analytes including explosives.[7] Rubinstein *et al.* showed that the LSPR of Au-nanostructures provides structural information about its molecular-based coating.[8]

We demonstrate here that the combination of an AuNP sub-monolayer with a metal–organic network (MON)[9] results in surface-confined core–shell nanostructures[10] (AuNP-MONs) with enhanced optical absorption of both components (Scheme 1). Our MON assembly strategy is compatible with the different surfaces in a single setup. The metallic nanoparticles' and the organic monolayer

[a] Department of Organic Chemistry, Weizmann Institute of Science, 76100, Rehovot, Israel. E-mail: milko.vanderboom@weizmann.ac.il

[b] Department of Physics and Astronomy and Department of Materials Science and Engineering, Northwestern University, Evanston, IL 60208, USA

[c] Dipartimento di Scienze Chimiche, Università di Catania, Catania 95125, Italy

† Electronic supplementary information (ESI) available: Experimental procedures and characterization data. See DOI: 10.1039/c3cc47865c
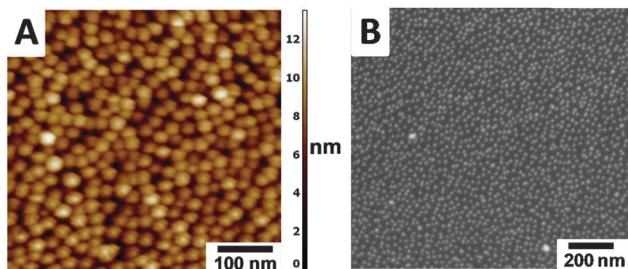
Scheme 1 Schematic illustration of the stepwise formation of the surface-confined core–shell nanostructures (**AuNP-MON**) on a pyridyl-terminated monolayer (Scheme S1, ESI†)[9] covalently bound to glass or silicon substrates.

surface were simultaneously functionalized with the **MON**. The use of the AuNPs resulted in an ordered **MON**, which is essentially a continuous shell embedding numerous cores.

Citrate-capped AuNPs (11.8 ± 1.3 nm, measured by transmission electron microscopy; TEM) were attached to glass and silicon substrates functionalized with a pyridyl-terminated monolayer (Scheme 1 and Scheme S1, ESI†). These surface-confined AuNPs were characterized using UV/vis spectroscopy, ellipsometry, scanning electron microscopy (SEM), and atomic force microscopy (AFM). A LSPR band at $\lambda_{max} = 516$ nm was observed by UV/vis spectroscopy, indicating that the citrate-capped AuNPs have a diameter of ~12 nm (Fig. S1 and S2, ESI†).[11] Ellipsometry measurements showed significantly different ψ and Δ parameters for the pyridyl-terminated monolayer before and after decoration with AuNPs (Fig. S3, ESI†). These changes are expected for a large increase in the film thickness.[12,13] Both SEM and AFM analyses indicated a surface coverage with mainly individual and spherical AuNPs having an average interparticle distance of ~27 nm (Fig. 1). The SEM-derived AuNP surface coverage is ~16%. The UV/vis spectroscopy, AFM, and SEM measurements indicate that there is no evident change in the AuNPs' dimensions, shape, and singularity when going from a solution to surface-bound AuNPs. The AuNPs bind to the pyridyl-terminated surface and do not aggregate due to the interparticle electrostatic repulsion of the negatively charged citrate capping layer.[14] The low AuNP coverage indicates that both

Fig. 1 AuNPs on silicon functionalized with a pyridyl-terminated monolayer (Scheme S1, ESI†).[9] (A) AFM image; the convolution limitation of the tip resulted in an overestimation of the AuNP diameter (Fig. S4, ESI†).[17] (B) SEM image showing an average AuNP distance of $\sim$27 nm.

the pyridyl-terminated monolayer and the surface of the AuNPs are available for forming the **MON**. Ligands such as **1**[15] can bind to citrate-capped AuNPs in solution, resulting in the formation of aggregates.[16]

The **AuNP-MONs** were obtained by an iterative deposition process of PdCl$_2$ and **1** on the AuNP platform (Scheme 1). No stabilization treatments were needed and the AuNP-functionalized substrates were used as is for the **MON** formation. The substrates were immersed in a THF solution of **1** (1.0 mM) for 15 min. Next, the samples were sonicated repeatedly in common organic solvents and dried under a stream of N$_2$. Subsequently, the samples were immersed in a THF solution of PdCl$_2$(PhCN)$_2$ (1.0 mM; 15 min), and then sonicated in the same manner as was the **1**-terminated layer. These two depositions were repeated 8 times to create the shell structure. Previously we formed **MON**s directly on pyridyl-terminated monolayers in the absence of AuNPs (Fig. 2 inset, Fig. S1, ESI†).[9]

The UV/vis spectra of the **AuNP-MONs** were recorded after each chromophore (**1**) deposition step (Fig. 2). Each step resulted in increased absorption intensities for both the LSPR band (λ_{max} = 516–554 nm) and the chromophore band ($\lambda_{max} \approx$ 335 nm). This latter absorption band is $\sim$3$\times$ higher (after subtracting the AuNP absorption) than the band of the **MON** grown directly on the

pyridyl-terminated monolayer.[9] This significant difference most likely results from the large surface area generated by the AuNPs. Taking into consideration the surface area of the AuNPs (450 nm^2 per AuNP) and their coverage (16%), the total surface area is enhanced by $\sim$1.5$\times$. Part of the AuNP surface is bound to the pyridyl-terminated monolayer and is not available for **MON** binding. Another factor contributing to the absorption intensity increase might involve energy transfer between the AuNP plasmon and molecular excitons.[18] Intermolecular interactions are not apparent but cannot be excluded for this type of chromophores.[9] The maximum position of the chromophore band is red shifted by only 9 nm for **AuNP-MON** having 9 layers of **1**. The deposition of the PdCl$_2$ salt has less effect on the optical signature of the **AuNP-MON** (Fig. S2, ESI†).

The **MON** formation on the AuNPs platform changes its effective dielectric media.[13] This change is shown by a red shift of the AuNP absorption band ($\Delta\lambda_{max}$ = 38 nm) and an intensity increase (3.3$\times$) of the characteristic LSPR band after the deposition of 8 chromophore layers. However, the changes in these optical properties level-off after 6 chromophore depositions (Fig. 3A and B), demonstrating that the influence of the **MON** thickness on the AuNP optical properties is significant up to $\sim$4 nm. A linear correlation was observed between the absorbance of the LSPR band and its wavelength (λ_{max}) (Fig. 3C).

X-ray photoelectron spectroscopy (XPS) is an established method to derive detailed information of metal–organic assemblies.[8,9,19a–c,24] Our angle-resolved XPS measurements revealed an elemental Pd/N
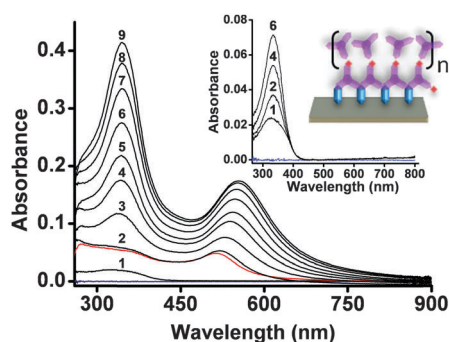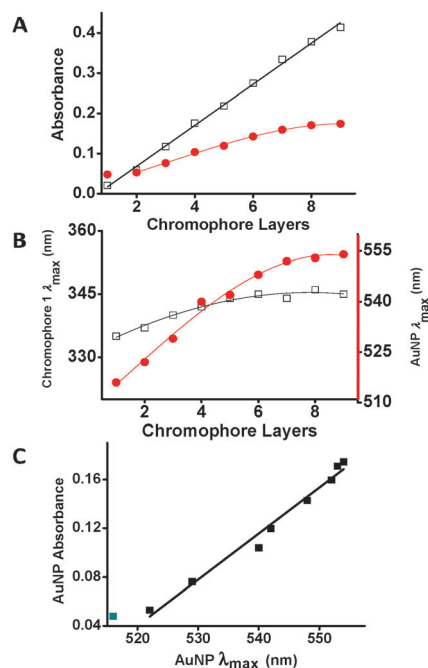

Fig. 2 UV/vis spectra showing the stepwise formation of **AuNP-MON** on a glass substrate. The first absorption spectrum (1) corresponds to the pyridyl-terminated monolayer (Fig. S2, ESI†). The red spectrum corresponds to the AuNP sub-monolayer (Scheme 1). Spectra 2–9 were recorded after each deposition of **1**. Inset: UV/vis absorption spectra taken from ref. 9 with $\lambda_{max} \approx$ 335 nm and a schematic illustration of the **MON** in the absence of the AuNPs. Data are shown for chromophore deposition steps 1, 2, 4, and 6. The baselines (blue) were recorded using bare slides.

Fig. 3 (A) The absorption maxima of **1** (□) and the AuNP band (●) vs. the deposition of **1**. The first red dot denotes the AuNP absorption prior to **MON** formation. The black line denotes a linear fit (R^2 = 0.99); the red line is a guide to the eye. (B) Position (λ_{max}) of the chromophore band (□; left axis) and surface plasmon (●; right axis) vs. the number of chromophore depositions. (C) Linear correlation between the absorption maxima of the AuNPs and its wavelength (λ_{max}) (R^2 = 0.98). The green dot of the AuNPs before chromophore deposition is excluded from the fit.
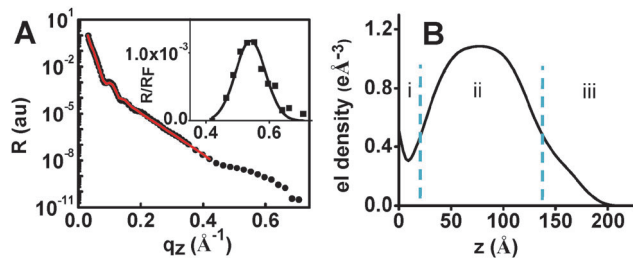
Fig. 4 (A) X-ray reflectivity (XRR) measurements of **AuNP-MON** on a silicon substrate (after 6 depositions of **1**). The red trace is a fit. Inset: a Bragg peak (normalized to the Fresnel reflectivity) after baseline subtraction can be discerned at $q_z \sim 0.54$ Å^{-1}. (B) Electron density profile (by Parratt fitting) as a function of the distance from the substrate surface.

ratio of ~ 0.53 for takeoff angles in the range $5–80°$ for **AuNP-MON** (after 6 chromophore depositions; Table S1, ESI†). A similar Pd/N ratio (0.54) was observed for the **MON** formed without the AuNPs.[9] These observations are in agreement with the formation of homogeneous structures with quantitative pyridine–palladium–pyridine coordination. The expected Pd/N ratio for a fully formed coordination network is 0.5. Ligands such as **1** form square-planar complexes by coordination of the pyridine moieties to PdCl$_2$ in a *trans*-configuration.[9] Interestingly, the XPS spectra showed the Au $4f_{7/2}$ and $4f_{5/2}$ signals at 83.2 and 86.9 eV, respectively. These binding energy values are relatively low,[19d,e] which is in good agreement with coordination of chromophore **1**. The C 1s spectrum does not show the presence of the citrate ligand (~ 289 eV) indicating an efficient capping layer exchange process. Deconvolution of the N 1s signal showed a main peak at 400.1 eV (N–Pd, N) and smaller peaks at 401.9 eV (N$^+$) and at 398.9 eV (N–Au). The ratio between these three peaks is $12:2:1$ and the ratio N$^+$:N–Au of $2:1$ reflects the contribution of the AuNPs to the overall surface area. These data correlate well with the AFM and SEM results. The presence of the pyridyl moieties was also indicated by Raman spectroscopy. Two peaks were observed at 1605 cm^{-1} and 1637 cm^{-1} corresponding to the C=C and pyridine groups.

In order to obtain additional structural information, specular X-ray reflectivity (XRR) measurements were performed for **AuNP-MON** after 6 chromophore depositions. The experimental data were fitted by applying the recursive Parratt algorithm (Fig. 4A).[20] The electron density profile obtained by this fit (Fig. 4B) indicates a 3-component system with a total thickness of 17 nm: (i) the pyridyl-terminated monolayer of ~ 2 nm thickness, (ii) the AuNPs with a diameter of ~ 12 nm, and (iii) the **MON**-shell with a thickness of ~ 3 nm. The observed electron density for the AuNP platform is 1.08 e Å^{-3} (Fig. 4B), while the electron density for AuNPs is 4.66 e Å^{-3}. Hence, the estimated electron density of the **MON** between the AuNPs is ~ 0.30 e Å^{-3} (using the AuNPs coverage of 16%; see ESI†). This estimate is in agreement with the results shown in Fig. 4B (section i). A Bragg peak was indicated at $q_z \sim 0.54$ Å^{-1}, with repeating distances of 1.2 nm and a correlation length of ~ 5.5 nm. These observations may imply that the **1**/PdCl$_2$ layers of the **MON** are organized with a certain periodicity.[21] We reported ordered molecular-based multilayers by combining coordination chemistry with π–π interactions.[22] Tao showed that Au nano-islands coated with a monolayer induced the formation of organized films.[4]

Here the molecular order is induced by the AuNPs. Without AuNPs, no Bragg peak was indicated.[9]

The ellipsometry-derived **AuNP-MON** thickness increased linearly with the number of deposition steps of **1** (Fig. S6, ESI†).[12,13] The final thickness (16 nm) is in agreement with the XRR data (Fig. S7, ESI†). SEM and AFM analyses indicated that the AuNPs are structurally not affected by the **MON** (Fig. 1, Fig. S8 and S9, ESI†).

To conclude, we have demonstrated the formation of a surface-confined core–shell nanostructure based on AuNPs and a **MON**. The AuNP cores have two major effects on the continuous shell: (i) the optical absorption intensity of the chromophores is positively affected by the larger surface area. The enhancement is higher than what one can expect based on only surface roughness considerations. Effects such as core–shell energy transfer[18] might also play a role. The AuNP plasmon band is affected by the thickness of the **MON** since it is sensitive to changes in the surrounding media. (ii) The use of the AuNP platform results in an ordered **MON**. Our findings demonstrate the long-range structural effects induced by nanostructures.[3,23] The large number of known coordination-based films[24] and the availability of surface-confined nanoparticles may make our approach a new entry for developing a wide range of composite interfaces.

Notes and references

1 B. Liu, O. Shekhah, H. K. Arslan, J. Liu, C. Wöll and R. A. Fischer, *Angew. Chem., Int. Ed.*, 2012, **51**, 807.
2 (*a*) Q. Gan, F. J. Bartoli and Z. H. Kafafi, *Adv. Mater.*, 2013, **25**, 2385; (*b*) Y. Xiao, F. Patolsky, E. Katz, J. F. Hainfeld and I. Willner, *Science*, 2003, **299**, 1877.
3 R. J. Macfarlane, B. Lee, M. R. Jones, N. Harris, G. C. Schatz and C. A. Mirkin, *Science*, 2011, **334**, 204.
4 C. W. Tseng and Y. T. Tao, *J. Am. Chem. Soc.*, 2009, **131**, 12441.
5 K. Ariga, Q. Ji, J. P. Hill, Y. Bando and M. Aono, *NPG Asia Mater.*, 2012, **4**, e17; O. Crespo-Biel, B. J. Ravoo, D. N. Reinhoudt and J. Huskens, *J. Mater. Chem.*, 2006, **16**, 3997.
6 (*a*) Y. Jin and N. Friedman, *J. Am. Chem. Soc.*, 2005, **127**, 11902; (*b*) J.-L. Wu, F.-C. Chen, Y.-S. Hsia, F.-C. Chien, P. Chen, C.-H. Kuo, M. H. Huang and C.-S. Hsu, *ACS Nano*, 2011, **5**, 959.
7 M. R. Jones, K. D. Osberg, R. J. Macfarlane, M. R. Langille and C. A. Mirkin, *Chem. Rev.*, 2011, **111**, 3736.
8 I. Doron-Mor, H. Cohen, Z. Barkay, A. Shanzer, A. Vaskevich and I. Rubinstein, *Chem.–Eur. J.*, 2005, **11**, 5555.
9 R. Kaminker, L. Motiei, A. Gulino, I. Fragalà, L. J. W. Shimon, G. Evmenenko, P. Dutta, M. A. Iron and M. E. van der Boom, *J. Am. Chem. Soc.*, 2010, **132**, 14554.
10 Y. Wei, S. Han, D. A. Walker, P. E. Fuller and B. A. Grzybowski, *Angew. Chem., Int. Ed.*, 2012, **51**, 7435.
11 S. Link and M. A. El-Sayed, *J. Phys. Chem. B*, 1999, **103**, 4212.
12 H. L. Zhang, S. D. Evans and J. R. Henderson, *Adv. Mater.*, 2003, **15**, 531.
13 S. Kubo, A. Diaz, Y. Tang, T. S. Mayer, I. C. Khoo and T. E. Mallouk, *Nano Lett.*, 2007, **7**, 3418.
14 D. A. Walker, B. Kowalczyk, M. O. de la Cruz and B. A. Grzybowski, *Nanoscale*, 2011, **3**, 1316.
15 A. J. Amoroso, A. M. W. C. Thompson, J. P. Maher, J. A. Mccleverty and M. D. Ward, *Inorg. Chem.*, 1995, **34**, 4828.

16 R. Kaminker, M. Lahav, L. Motiei, M. Vartanian, R. Popovitz-Biro, M. A. Iron and M. E. van der Boom, *Angew. Chem., Int. Ed.*, 2010, **49**, 1218; L. Beverina, *ChemPhysChem*, 2010, **11**, 2075.
17 A. Doron, E. Joselevich, A. Schlittner and I. Willner, *Thin Solid Films*, 1999, **340**, 183.
18 K. O. Aruda, M. Tagliazucchi, C. M. Sweeney, D. C. Hannah and E. A. Weiss, *Phys. Chem. Chem. Phys.*, 2013, **15**, 7441.
19 (*a*) A. Gulino, *Anal. Bioanal. Chem.*, 2013, **405**, 1479; (*b*) S. L. Tait, Y. Wang, G. Costantini, N. Lin, A. Baraldi, F. Esch, L. Petaccia, S. Lizzit and K. Kern, *J. Am. Chem. Soc.*, 2008, **130**, 2108; (*c*) I. Doron-Mor, A. Hatzor, A. Vaskevich, T. van der Boom-Moav, A. Shanzer, I. Rubinstein and H. Cohen, *Nature*, 2000, **406**, 382; (*d*) M. P. Seah,

L. S. Gilmore and G. Beamson, *Surf. Interface Anal.*, 1998, **26**, 642; (*e*) N. H. Turner and A. M. Single, *Surf. Interface Anal.*, 1990, **15**, 215.
20 (*a*) C. Braun, *Parratt32 Software for Reflectivity*, HMI, Berlin, 1999; (*b*) L. G. Parratt, *Phys. Rev.*, 1954, **95**, 359.
21 B. Wedl, R. Resel, G. Leising, B. Kunert, I. Salzmann, M. Oehzelt, N. Koch, A. Vollmer, S. Duhm, O. Werzer, G. Gbabode, M. Sferrazza and Y. Geerts, *RSC Adv.*, 2012, **2**, 4404.
22 M. Altman, O. Zenkina, G. Evmenenko, P. Dutta and M. E. van der Boom, *J. Am. Chem. Soc.*, 2008, **130**, 5040.
23 S. J. Tan, M. J. Campolongo, D. Luo and W. Cheng, *Nat. Nanotechnol.*, 2011, **6**, 268.
24 I. Rubinstein and A. Vaskevich, *Isr. J. Chem.*, 2010, **50**, 333.